Inversion of 3D time-domain electromagnetic data: the effect of time-weighting

Marwan Wirianto, Shell Global Solutions International and Delft University of Technology,*
R.-E. Plessix, Shell Global Solutions International, and
W. A. Mulder, Shell Global Solutions International and Delft University of Technology

SUMMARY

In order to mitigate the airwave problem, caused by the interaction between source-excited electromagnetic fields and the air, controlled-source electromagnetic surveys on land are almost exclusively implemented as a transient electromagnetics system (TEM), typically measuring step-off or step-on responses. In this way, the earth response can be well separated from the air response, as the latter primarily arrives at very early times and is then followed by the earth response. Because the air response carries no information about deeper targets, the early-time data are often considered useless and are removed in processing and inversion. In this paper, we show that simply muting the early-time TEM data may lead to unsatisfactory inversion results. Without the early-time response, inversion cannot retrieve the resistivity of the near surface. Due to the diffusive nature of the electromagnetic fields, this also affects the recontruction of the resistivity at larger depths. We illustrate this with a synthetic example.

INTRODUCTION

The controlled-source electromagnetics (CSEM) method is considered to be a useful geophysical tool for oil and gas exploration (Ellingsrud et al., 2002). The reason is that CSEM data can provide resistivity maps of the subsurface, hence may allow us to estimate the prospect resistivity, thereby reducing the exploration risk in finding commercial hydrocarbon deposits. Nowadays, the CSEM method is widely used in deep marine, shallow water, and land environments.

Acquisitions with the CSEM method can principally be subdivided into frequency-domain (FDEM) and time-domain (TEM) systems. In frequency-domain systems, we typically measure electromagnetic signals generated by a periodic, alternating source current that employs one or a few frequencies. In TEM systems, we measure electromagnetic signals induced by a certain combination of step-on or step-off source currents, repeated several times and stacked together to improve the signal-to-noise ratio. FDEM systems are preferably used in deep-marine environments where the thick layer of sea water effectively shields the measurements from EM noise present at the surface, whereas TEM systems are more appropriate in shallow water and on land because of the much stronger EM noise.

The interaction between the source-excited EM fields and the air creates a source-induced airwave component. This airwave may dominate the EM field measurements at any frequency, making the signal from the subsurface hard to distinguish in a frequency-domain approach. The airwave propagates in the air with the speed of light, whereas the electromagnetic fields diffuse into the earth. The part that propagates along the surface is called a lateral wave. It sends an electromagnetic field into the ground with an almost vertical diffusion direction (Baños, 1966; King et al., 1992). A similar effect can be observed for a source at the interface between two conducting layers, where the fast diffusive medium (low conductivity) generates a field in the slow diffusive medium (high conductivity) that diffuses in the direction of the normal to the interface. With step-off or step-on sources in a TEM system, the earth response can generally be well separated from the air response in the time domain, since the latter, propagating with the speed of light, primarily arrives at a very early time and is then followed by the earth response. Hence, in the processing we could boost the late-time data to extract the information of the deeper targets.

The TEM signal that carries deep-target information is often weaker than the EM noise. Measurements need to be repeated and stacked together to obtain TEM data with a good enough signal-to-noise ratio. After this acquisition procedure, the earth response can generally be well separated from the air response. This time separation requires a large enough frequency band, otherwise the signal is not sufficiently localized in time. This means that measuring the data misfit between modeled and observed data in the frequency domain is not well suited for inversion. A time-domain formulation is preferred. However, the interpretation of measured TEM data can still be difficult. As the early-time data carry no information about deeper targets, they are often considered useless and removed in processing and inversion. However, this may harm the resistivity estimate. Muting the early-time responses may remove information about the shallow resistivity variations. In the later time responses, shallow and deep resistivity variations are mixed because of the strongly diffusive nature of electromagnetic signals in the earth.

In this paper, we study the early-time muting of TEM data in a time-domain inversion scheme. We investigate some time weighting approaches and their effect on the final resistivity images. We first explain the implementation of the time-domain inversion. For efficiency, the time-domain responses are obtained by Fourier transforms of a limited number of frequency-domain responses, using a logarithmic fast-Fourier transform. Then, we present an example showing that simply muting the early times of TEM data can lead to unsatisfactory results.

METHOD

We formulate the resistivity imaging of TEM data as an inverse problem. With the observed electric and magnetic time series, $\mathbf{e}^{\text{obs}}_{s,r}(t)$ and $\mathbf{h}^{\text{obs}}_{s,r}(t)$, generated at the source positions $\mathbf{x}_s$ and observed at the receiver positions $\mathbf{x}_r$, the inverse problem consists of finding a resistivity ρ that minimizes the weighted

© 2011 SEG

least-squares functional

$$J(\rho) = \frac{1}{2}\sum_s \sum_r \int_0^T \left\{ \|w^e_{s,r}(t)\Delta\mathbf{e}_{s,r}(t;\rho)\|^2 + \|w^h_{s,r}(t)\Delta\mathbf{h}_{s,r}(t;\rho)\|^2 \right\} dt \quad (1)$$

where

$$\Delta\mathbf{e}_{s,r}(t;\rho) = \mathbf{e}_{s,r}(t;\rho) - \mathbf{e}^{\text{obs}}_{s,r}(t), \quad \text{and}$$
$$\Delta\mathbf{h}_{s,r}(t;\rho) = \mathbf{h}_{s,r}(t;\rho) - \mathbf{h}^{\text{obs}}_{s,r}(t).$$

Here, T is the maximum recording time, $\mathbf{e}_{s,r}$ and $\mathbf{h}_{s,r}$ represent the computed electric and magnetic responses, and $w^e_{s,r}$ and $w^h_{s,r}$ are data weights depending on source and receiver locations and time.

Following closely the approach of Plessix and Mulder (2008), we minimize J in equation 1 with a quasi-Newton optimization, a limited-memory version of the Broyden-Fletcher-Goldfard-Shanno (BFGS) method (Byrd et al., 1995). We follow the classic inverse problem formulation where the gradient of the least squares functional is computed with the adjoint method. We apply a regularization term in order to stabilize the optimization process. As with each gradient-based optimization, our approach requires an efficient 3D numerical solver. In the following paragraph, we describe how we tackle this issue.

For time-domain EM modeling, there are a number of options. The most prominent methods are explicit Du Fort-Frankel time-stepping schemes, implicit schemes, Lanczos-based reduction and matrix exponential schemes, and Fourier-transform-based methods. However, by comparing the computational complexity of these methods, Mulder and Slob (2007) show that frequency-domain modeling followed by a Fourier transformation is an attractive choice. The computational cost of a time-domain solution with this approach is determined mostly by the number of frequencies. With parallel computers, this leads to an efficient solver for time-domain EM modeling since different frequencies can be treated simultaneously. Here, we adopt this approach. The frequency responses are computed with an efficient iterative method preconditioned by one cycle of a multigrid solver (Mulder, 2006).

The choice of the frequency discretization remains to be decided. Because of the diffusive nature, it is generally recognized that a time-domain EM response is well represented by a set of frequencies on a regularly spaced logarithmic frequency axis. Since we need to compute the responses over a large frequency band, say between 0.01 and 100 Hz, a logarithmic scale saves a considerable amount of computations compared to a linear scale. Mulder et al. (2008), for instance, used an approach that consists of computing the responses on a set of frequencies regularly spaced on a logarithmic axis, then interpolating the responses with cubic Hermite interpolation to a set of frequencies regularly spaced on a linear axis, and finally computing the time-domain response with a standard Fast Fourier Transformation (FFT). This approach is a simple and straightforward. However, the use of the standard FFT for time-domain EM modeling is rather costly. FFT requires a dense sampling in order to capture the early-time data, (namely the high frequencies), which increases the number of points and makes the standard FFT expensive. The use of a Fourier transform on a logarithmic axis is therefore an attractive choice, which we adopt here (Talman, 1978; Haines and Jones, 1988). Our implementation is as follows. First, we compute the frequency responses on a regularly spaced logarithmic frequency axis, then we determine the time responses with a logarithmic Fourier transform. The resulting time responses are discretized on a regularly spaced logarithmic time axis. Finally, we interpolate the time responses on a regularly spaced linear time axis with cubic Hermite interpolation.

RESULTS

Modeling test

We start by showing the relevance of our modeling approach by comparing our estimated time response with the exact analytical solution. We consider a homogeneous half-space model with a resistivity of 0.5 Ωm. The source is an in-line electrical point dipole source placed on the surface. Three receivers are placed on the surface at $(x,y) = (0,2)$ km, $(2,2)$ km, and $(5,2)$ km, respectively, measuring the in-line electric field. The time-domain solution is sampled at a rate of 0.01 s within the range $[0,100]$ s.

The results are displayed in Figure 1. The red dots represent the solutions computed with the standard FFT. In this approach, the interpolation to a regular linear sampling is done in the frequency domain. The blue dots represent the solutions with the logarithmic FFT. Now, the interpolation to a regular linear sampling is done in the time domain. For comparison, we have plotted the exact analytical solution with black lines. Although some inaccuracies are visible at very late times, the use of the logarithmic Fourier transformation clearly provides more accurate solutions at the early and late times compared to the ones obtained by standard FFT. In this test, we have used the same number of frequency-domain responses in both approaches. To obtain a better results with the standard FFT approach, a much larger numbers of frequency-domain responses would need to be evaluated. This would considerably increase the computational time.

Inversion problem

We carried out a small synthetic time-domain inversion. The time-domain responses were computed with the multigrid-based frequency-domain solver and the logarithmic FFT as explained in the previous section. The "true" model consists of a 0.5 Ωm half-space background resistivity and a 100 Ωm resistor located at 1 km depth below the surface. The dimension of the resistor is 2 km by 2 km by 100 m. The top panel of Figure 3 shows a vertical cross section of the resistivity model. The acquisition geometry is displayed in Figure 2. We consider three receiver lines with a 1 km spacing between the lines. Each lines contains 32 receivers spaced at 200 m. Only the in-line electric components are recorded. We considered 2 source positions with a spacing of 4 km. Each source is laterally located at 1 km from the edge of hydrocarbon target. The maximum recording time is 10 s and the sampling rate 0.01 s.

© 2011 SEG

Time-domain inversion

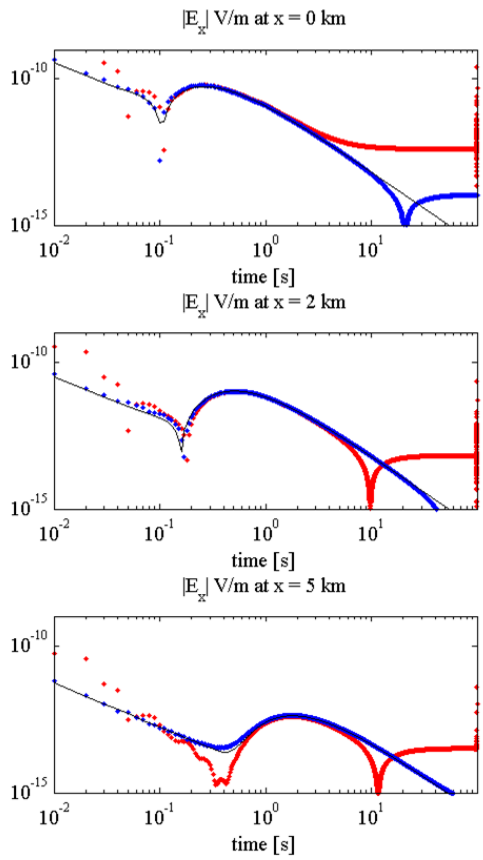

Figure 1: Time response of E_x, generated by an x-directed point source located at the origin of the model on the surface. The three receivers are also located on the surface with the following lateral coordinates $(x,y) = (0,2)$ km (top), $(2,2)$ km (middle), and $(5,2)$ km (bottom). The red dots corresponds to the estimated solution with the standard FFT, the blue dots to the solution when with the logarithmic Fourier transformation, and the black line to the exact analytical solution.

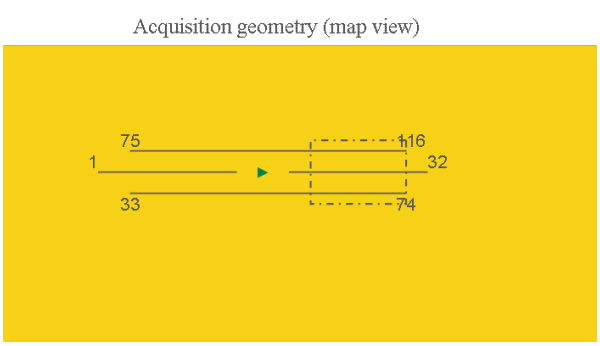

Figure 2: The dash line indicates the lateral position of hydrocarbon target. The green triangle indicates the lateral position of a source. Solid lines show the receiver configuration, consisting of 32 receivers per line. Numbers indicates receiver indexes. Receivers 1–32 are placed in an in-line configuration, while 33–74 and 75–116 have a broad-side configuration.

For the first inversion example, we take the full time responses into account, including early and late times. The initial model is a 0.5 Ωm homogeneous half-space resistivity model. We did not apply any data weights or depth weighting. The top panel of Figure 4 shows the normalized difference between the data and the computed responses with the initial resistivity model. A large anomaly can be observed between 0.1 s and 2 s for the receivers located above the target.

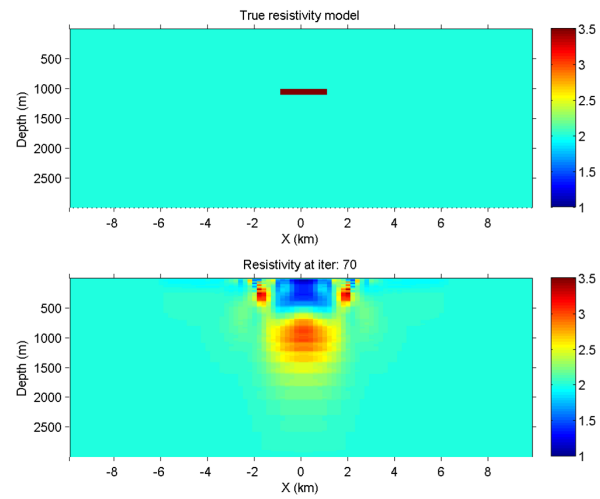

Figure 3: The bottom panel shows the optimal resistivity model after 70 iterations, while the top panel shows the true model used to generate data. The resistivity values are clipped at 3.5 Ωm

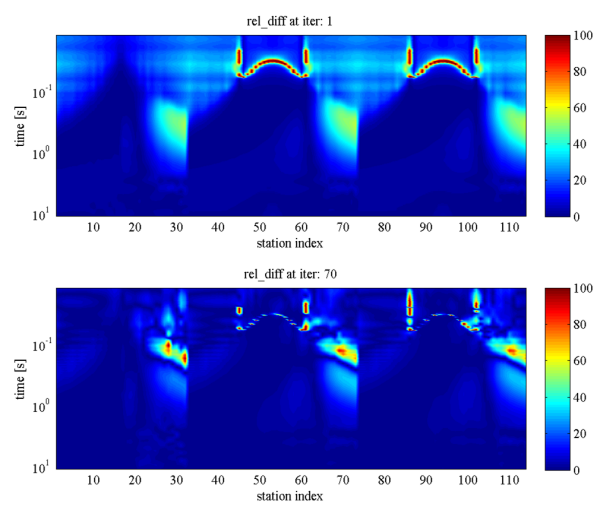

Figure 4: The normalized misfit between the data and the computed responses. The scale is in percent.

The final resistivity model, plotted in the bottom panel of Figure 3, was obtained after 70 iterations. The deep resistive zone is well retrieved. Due to the diffusive nature of the EM inversion, the resolution is poor, as expected. The final normalized data misfit is shown in the bottom panel of Figure 3. The misfit is significantly reduced, indicating that the final model correctly

© 2011 SEG

interprets the data. Some overshoots in the final normalized differences are due to division by small numbers. A single inversion iteration took a bit more than 30 minutes, computing 40 frequencies in parallel on 40 cores, and required 80 forward and 40 backward modeling steps. We needed twice the number of forward computations, because we did not store the forward fields for the gradient. Instead, after having computed the data residual, we recomputed the forward fields for the correlation with the backward fields. The convergence rate of the inversion may be sped up by applying suitable depth and data weighting, but we did not consider that here.

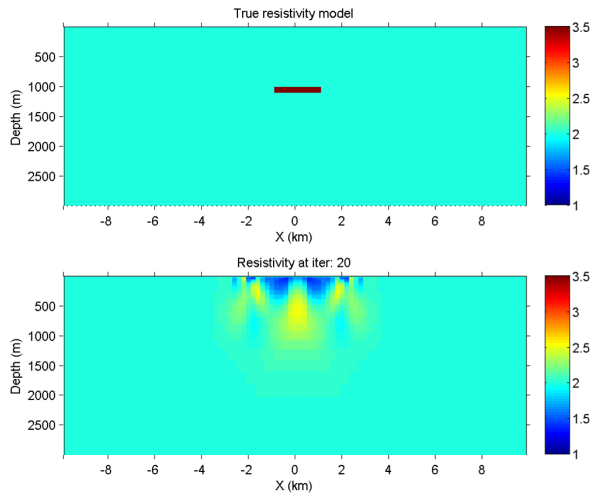

Figure 5: The bottom panel shows the resistivity model after 20 iterations, while the top panel shows the true model used to generate data. The resistivity values are clipped at 3.5 Ωm

The effect of time weighting

The previous result shows that the resistivity model can be well retrieved with a time-domain EM inversion and the full time series. In real cases, using the early times may not be possible. The airwave may not be correctly sampled or its amplitude may be clipped. In a second inversion, we investigate the effect of removing/blanking the early times. We use the same dataset as in the previous example. Because the large anomaly coming from the deep resistor was observed after 0.1 s, we decided to mute the data from 0 to 0.1 s, as shown in in Figure 6 by a yellow box. Then, we ran the inversion with the same parameters as the previous example. The data misfit decreased very slowly. We stopped the inversion after 20 iterations. The bottom panel of Figure 5 shows the resistivity model and the bottom panel of Figure 6 shows the normalized data misfit. We notice that the inversion starts to explain the data for late times. However, significant shallow artifacts appear in the resistivity map. Removing the early-time data makes the non-uniqueness of the inversion worse. It apparently enlarges the null space of the misfit function. In the previous inversion, the early times helped to constrain the shallow part of the resistivity. Because of the diffusive nature of the electromagnetic fields, there is a trade-off between the shallow and deep part of the model. When the shallow part cannot be correctly constrained or estimated, the deep part is not retrieved satisfactory. This behaviour is somewhat similar to the static shift phenomena common to EM measurements. A local high-resistivity contrast in the near surface biases the interpretation of the resistivity in the deeper part of the earth.

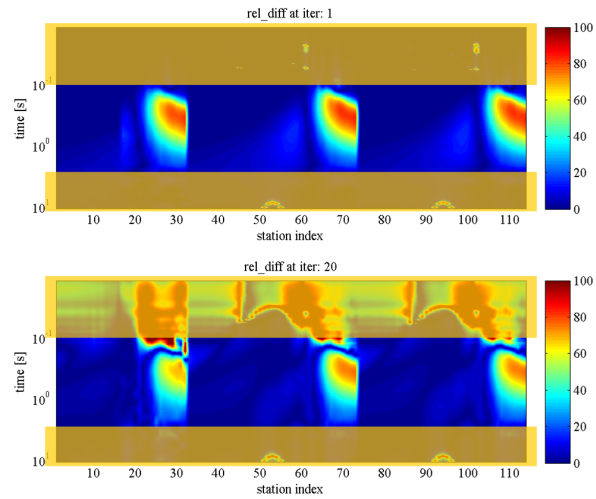

Figure 6: The normalized data misfit. The yellow box indicates data clipping. The scale is in percent.

CONCLUSION AND FUTURE OUTLOOK

We have studied some effects of time weighting on time-domain EM inversion. The results show that simply muting the early-time TEM data may lead to unsatisfactory results because it makes the non-uniqueness worse. Inversion cannot retrieve the resistivity of the near surface, which makes the interpretation of the resistivity map at depth difficult, if not impossible. The use of offset and depth weighting may mitigate this problem. However, not constraining or estimating the shallow part of the resistivity model may bias the results.

ACKNOWLEDGMENTS

The authors thank Shell for permission to publish this paper and Mathieu Darnet and Peter van der Sman for their support.

© 2011 SEG

EDITED REFERENCES

Note: This reference list is a copy-edited version of the reference list submitted by the author. Reference lists for the 2011 SEG Technical Program Expanded Abstracts have been copy edited so that references provided with the online metadata for each paper will achieve a high degree of linking to cited sources that appear on the Web.

REFERENCES

Baños, A., 1966, Dipole radiation in the presence of a conducting half-space: Pergamon Press, Inc.

Byrd, R. H., P. Lu, J. Nocedal, and C. Zhu, 1995, A limited memory algorithm for bound constrained optimization: SIAM Journal on Scientific Computing, **16**, 1190–1208, doi:10.1137/0916069.

Ellingsrud, S., T. Eidesmo, S. Johansen, M. C. Sinha, L. M. MacGregor, and S. Constable, 2002, The meter reader: Remote sensing of hydrocarbon layers by seabed logging (SBL): Results from a cruise offshore Angola: The Leading Edge, **21**, 972–982, doi:10.1190/1.1518433.

Haines, G. V., and A. G. Jones, 1988, Logarithmic Fourier transformation: Geophysical Journal, **92**, 171–178, doi:10.1111/j.1365-246X.1988.tb01131.x.

King, R. W. P., M. Owens, and T. T. Wu, 1992, Lateral electromagnetic waves: Theory and applications to communications, geophysical exploration, and remote sensing: Springer-Verlag.

Mulder, W. A., 2006, A multigrid solver for 3D electromagnetic diffusion: Geophysical Prospecting, **54**, 633–649, doi:10.1111/j.1365-2478.2006.00558.x.

Mulder, W. A., and E. C. Slob, 2007, TDEM by FDEM: Proceedings of the Progress In Electromagnetics Research Symposium, 1794–1798.

Mulder, W. A., M. Wirianto, and E. C. Slob, 2008, Time-domain modeling of electromagnetic diffusion with a frequency-domain code: Geophysics, **73**, no. 1, F1–F8, doi:10.1190/1.2799093.

Plessix, R.-É., and W. A. Mulder, 2008, Resistivity imaging with controlled-source electromagnetic data: depth and data weighting: Inverse Problems, **24**, 034012, doi:10.1088/0266-5611/24/3/034012.

Talman, J. D., 1978, Numerical Fourier and Bessel transforms in logarithmic variables: Journal of Computational Physics, **29**, 35–48, doi:10.1016/0021-9991(78)90107-9.

© 2011 SEG